The Astrophysical Journal, 657:400–408, 2007 March 1

HARD X-RAY EMISSION OF THE MICROQUASAR GX 339−4 IN THE LOW/HARD STATE

A. Joinet,[1] E. Jourdain,[1] J. Malzac,[1] J. P. Roques,[1] S. Corbel,[2] J. Rodriguez,[2] and E. Kalemci[3]

Received 2006 June 26; accepted 2006 October 12

ABSTRACT

We present the analysis of the high-energy emission of the Galactic black hole binary GX 339−4 in a low/hard state at the beginning of its 2004 outburst. The data from 273 ks of *INTEGRAL* observations, spread over 4 weeks, are analyzed, along with the existing simultaneous *RXTE* HEXTE and PCA data. During this period, the flux increases by a factor of $\simeq$3, while the spectral shape is quite unchanged, at least up to 150 keV. The high-energy data allow us to detect the presence of a high-energy cutoff, generally related to thermal mechanisms, and to estimate the plasma parameters in the framework of the Comptonization models. We found an electron temperature of 60–70 keV and an optical depth of around 2.5, with a rather low reflection factor (0.2–0.4). In the last observation, we detected a high-energy excess above 200 keV with respect to thermal Comptonization, while at lower energies the spectrum is practically identical to the previous one taken just 2 days before. This suggests that the low- and high-energy components have a different origin.

Subject headings: accretion, accretion disks — black hole physics — gamma rays: observations — stars: individual (GX 339−4) — X-rays: binaries

Online material: color figures

1. INTRODUCTION

Since its discovery more than 30 years ago by Markert et al. (1973), the X-ray binary GX 339−4 has been extensively studied with several optical, infrared, X-ray, and γ-ray observatories. The optical companion is undetectable (Shahbaz et al. 2001), but upper limits on its luminosity allowed the source to be classified as a low-mass X-ray binary that could belong to the Galactic bulge (with $d_{\rm min} \gtrsim 6.7$ kpc; Zdziarski et al. 2004). Hynes et al. (2003) propose to classify GX 339−4 as a black hole with a mass function of 5.8 $M_\odot$.

The source has complex variability behavior with nearly persistent outbursting X-ray and γ-ray activity and the presence of quite long periods of quiescence (Kong et al. 2002). In the soft X-rays it was observed at high resolution with *Chandra* and *XMM-Newton* (Miller et al. 2004a, 2004b), while Belloni et al. (2005) reports on the source timing and color analysis. At higher energy its emission has been studied by all the major observatories, such as *Granat* SIGMA (Grebenev et al. 1993; Bouchet et al. 1993) and the *Compton Gamma Ray Observatory* (*CGRO*; Grabelsky et al. 1993). Zdziarski et al. (2004) present an extensive spectral analysis of the source covering the 1987–2004 period using *CGRO* BATSE, *Ginga* ASM, and *Rossi X-Ray Timing Explorer* (*RXTE*) data. Homan et al. (2005) present a coordinated multiwavelength study of the 2002 outburst and suggest a nonthermal/jet origin for the optical/near-infrared emission (Corbel & Fender 2002) in the hard state, while the accretion disk dominates in the soft state.

In transient Galactic black holes such as GX 339−4, the accretion rate varies by several orders of magnitude. They consequently exhibit a complex spectrotemporal variability. X-ray monitoring campaigns (with, e.g., *RXTE*) demonstrated the existence of two main X-ray spectral states. Sources are usually observed with a X-ray luminosity lower than a few percent of the Eddington luminosity in the so-called low/hard state (LHS), characterized by a relatively low flux in the soft X-rays ($\lesssim$1 keV) and a high flux in the hard X-rays ($\sim$100 keV). In the LHS, the high-energy spectrum can be roughly described by a power law with spectral index Γ varying in the range 1.4–2.1 and a nearly exponential cutoff at a few hundred keV (see, e.g., Gierliński et al. 1997). When the luminosity exceeds a few percent of the Eddington luminosity, the sources can switch to the high/soft state (HSS). The high-energy power law is then much softer ($\Gamma \geq 2.4$), without any hint of a high-energy cutoff, and the bolometric luminosity is dominated by the disk thermal component, peaking at a few keV. Beside the LHS and HSS, there are several other spectral states that often appear, but not always, when the source is about to switch from one of the two main states to the other. Those states are more complex and are difficult to define. We refer the reader to McClintock & Remillard (2006) and Belloni et al. (2005) for two different spectral classifications based on X-ray temporal, as well as spectral, criteria and radio emission (Fender 2006). The hard power-law plus cutoff spectrum of the LHS is usually interpreted as thermal Comptonization in a hot ($kT_e \sim 100$ keV) optically thin plasma (the corona). In addition to the dominant Comptonization spectrum, there are several other less prominent spectral features:

1. A weak soft component associated with the thermal emission of a geometrically thin, optically thick disk is occasionally detected below 1 keV, as observed in Cygnus X-1 (Balucinska-Church et al. 1995) or in XTE J1118+480 (McClintock et al. 2001; Chaty et al. 2003).
2. A Fe Kα line at $\sim$6.4 keV and a Compton reflection bump peaking at $\sim$30 keV are believed to be the signature of the irradiation of the cold, optically thick disk by the hard X-rays from the corona (George & Fabian 1991).
3. A high-energy ($\geq$200 keV) excess with respect to simple thermal Comptonization models was detected in GX 339−4 by the Oriented Scintillation Spectrometer Experiment (OSSE; Johnson et al. 1993) during the LHS of its 1991 outburst. A similar excess was detected by COMPTEL in the LHS of Cyg X-1 (McConnell et al. 2000). This excess is possibly produced by a tiny population of nonthermal electrons that could be part of the coronal plasma,

[1] Centre d'Etude Spatiale des Rayonnements, CNRS-UPS, Toulouse, France.
[2] Université Paris 7, Denis Diderot and Service d'Astrophysique, UMR AIM, CEA Saclay, Gif sur Yvette, France.
[3] Sabancı University, Orhanlı-Tuzla, İstanbul, Turkey.

TABLE 1
INTEGRAL Observations of GX 339−4

Rev.	INT_{start}	INT_{stop}	Δt_{sp} (ks)	ID	RX_{start}	RX_{stop}	Exp. (ks)
166.....	53057.07	53059.45	152	90109-01-01-00	53058.99	53059.17	16.1
167.....	53061.62	53062.22	40	80132-01-07-00	53061.75	53061.86	9.3
174.....	53080.99	53081.67	38	90118-01-06-00	53081.51	53081.54	2.8
175.....	53084.77	53085.45	43	80102-04-66-00	53084.46	53084.49	2.5

Notes.—For each *INTEGRAL* revolution ("Rev."), we give the beginning, INT_{start}, and the end, INT_{stop}, of the *INTEGRAL* observations, in MJD. The quantity Δt_{sp} is the useful duration for SPI observations, "ID" indicates the identification program number of *RXTE* observations, RX_{start} and RX_{stop} are the beginning and the end of the *RXTE* observations taken (quasi-)simultaneously with *INTEGRAL* observations, and "Exp." is the exposure time for PCA.

or not. With the *INTEGRAL* SPI, we have the opportunity to monitor the excess above 200 keV, which, as discussed in § 4, is crucial to be able to address the emission mechanism at these energies.

In this paper, we focus only on observations performed when GX 339−4 was in the LHS, while Belloni et al. (2006) study the evolution of the high-energy cutoff during the transition from the low/hard to the high/soft state. We present here the overall available *INTEGRAL* SPI+IBIS and simultaneous *RXTE* Proportional Counter Array (PCA) and High-Energy X-Ray Timing Experiment (HEXTE) data (see Table 1) that cover the rising phase of the 2004 outburst.

The analysis is based on the data registered from MJD 53057 (*INTEGRAL* revolution 166 on 2004 February 4) to MJD 53085 (*INTEGRAL* revolution 175 on 2004 March 21), limiting us to the low/hard state study. We briefly describe the *INTEGRAL* and *RXTE* telescopes, as well as data analysis methods, in § 2. The results, which concern mainly spectral evolution, are presented in § 3 and then discussed in § 4.

2. OBSERVATIONS AND DATA ANALYSIS

The first indication of a new reactivation of GX 339−4 was provided by Buxton et al. (2004), who reported a radio and optical source flux increase on 2004 February 4–5. Then on 2004 February 9, the X-ray activity was definitively renewed (Smith et al. 2004; Belloni et al. 2004), and the source was detected by *INTEGRAL* on 2004 February 19 (MJD 53054; Kuulkers et al. 2004). This paper is based on data taken during the first part of the outburst, when the source was in the hard state. Table 1 gives the details of each *INTEGRAL* revolution and corresponding quasi-simultaneous *RXTE* observations used in this analysis (i.e., for the LHS). Figure 1 shows the *RXTE* all-sky monitor (ASM) light curve of the source in the 1.5–12 keV energy range, together with *INTEGRAL* observation periods.

2.1. *INTEGRAL*

2.1.1. *SPI*

The spectrometer SPI (Spectrometer for *INTEGRAL*; Vedrenne et al. 2003; Roques et al. 2003) is dedicated to the spectral analysis of γ-ray point sources and extended regions in the 20 keV–8 MeV energy range. The detector plane features an array of 19 hexagonal high-purity Germanium crystals, operating at a temperature of 85 K. A hexagonal coded aperture mask is located 1.7 m above the detection plane in order to image the sky over a 16° (corner to corner) field of view, with an angular resolution of 2.5°. In order to reduce background radiation, the camera is shielded by a veto (anticoincidence) system that extends around the bottom and side of the detector plane almost completely up to the coded mask.

The *INTEGRAL* revolutions last $\simeq$3 days, during which the observations are realized through a combination of several 30–40 minute duration pointings, separated by 2° and covering the same sky region ("dithering strategy" see Jensen et al. 2003). While the number of SPI detectors (pixels) is small, this method increases the amount of data in excess of the number of unknowns for a better determination of the background and source fluxes.

INTEGRAL SPI data were reduced as explained in § 4.1 of Joinet et al. (2005), with the exception that only 18 detectors have been used, as detector 2 failed during revolution 140.

For each source, the timescale has been chosen on the basis of its intensity and its a priori known or observed temporal behavior. As the errors increase with the degrees of freedom, i.e., the number of considered temporal bins, it is important not to oversample the variability. See § 3 for the details.

We have checked that the background flux is stable within each of the considered revolutions. We have thus used only one normalization parameter per orbit, with an uniformity map determined for the 18 detector configuration.

The photon spectra have been constructed from the counts spectra in 19 energy bins and were deconvolved with the energy response matrix corresponding to each pointing (Sturner et al. 2003). We added a 3% systematic error to all spectral channels, and the spectra were fitted from 23 to 600 keV in XSPEC.

Only pointings for which GX 339−4 was at a distance lower than 12° from the central axis were taken into account for the

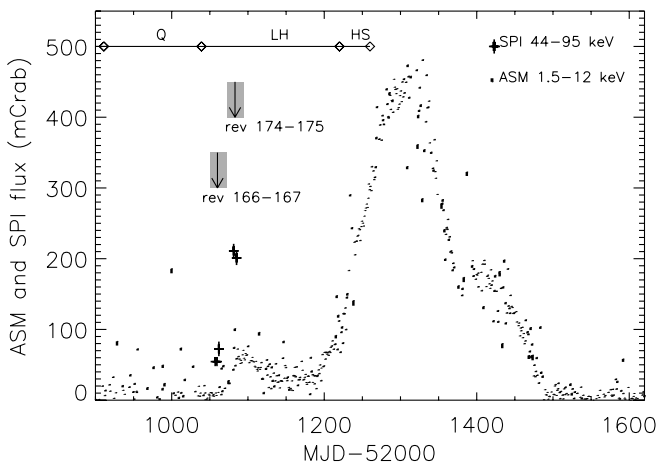

Fig. 1.—*RXTE* ASM and SPI light curves of GX 339−4, showing a quiescent period followed by the 2004 outburst. The different states harbored by the source are summarized on the graph as follows: Q: quiescent, LH: low/hard, and HS: high/soft (see Remillard 2005). The arrows represent the *INTEGRAL* observation periods (revolutions 166, 167, 174, and 175).

analysis. We excluded pointings affected by a solar flare or by exit/entry into the radiation belts. We obtained 273 ks of useful data with 140 pointings during the observation period covered by revolutions 166, 167, 174, and 175 (see Table 1).

2.1.2. *IBIS*

The Imager On Board *INTEGRAL* (IBIS) is a coded mask telescope with a total field of view of $29^\circ \times 29^\circ$ (down to 0 response) composed of a two-layer detection plane. We use here only data from the upper layer, the *INTEGRAL* Soft Gamma-Ray Imager (ISGRI; Lebrun et al. 2003). This detector is sensitive from $\sim$13 keV to $\sim$1000 keV. Due to its low efficiency and the general faintness of the fluxes of sources above $\sim$400 keV, it generally has a limited use above that energy.

The IBIS ISGRI has excellent imaging capabilities, with an angular resolution of $12'$ and a positional accuracy of $\sim 1'$, depending on a given source's signal-to-noise ratio. ISGRI also possesses spectral capabilities, although with a much poorer resolution than SPI, with $\Delta E/E \sim 0.1$ at 60 keV.

The data from IBIS ISGRI were reduced in a manner strictly identical to the one reported in Rodriguez et al. (2006), which focuses on the same field, with the exception that the latest version of the Offline Scientific Analysis (OSA) software (version 5.1) was used. To quickly summarize, we first produced images in two energy ranges (20–40 keV and 40–80 keV) to identify the most active sources. We then extracted spectra from all the sources in this field that had a detection significance higher than 7. We rebinned the original response matrix (`isgri_rmf_grp_0016.fits`) to 63 channels before the extraction. The latest time-dependent ancillary response file (`isgri_arf_rsp_0013.fits`) was then associated with the file for the spectral fits. We added 2% systematics to all spectral channels, and the spectra were fitted (together with those from the other instruments) from 25 to 200 keV.

2.2. *RXTE*

We also analyzed the public PCA and HEXTE (Bradt et al. 1993; Rothschild et al. 1998) data. Table 1 summarizes the set of *RXTE* observations performed contemporaneously with the *INTEGRAL* data observation periods.

We limited the energy range from 3 to 25 keV and from 25 to 200 keV for the PCA and HEXTE data, respectively. The data reduction was done using the FTOOLS routines in the HEAsoft software package distributed by NASA's HEASARC (version 5.2). We followed the steps of standard reduction as explained in the *RXTE* Cook Book.[4] The spectrum extraction was performed from data taken in "Standard 2" mode. The response matrix and the background spectra were created using FTOOLS programs. Background spectra were made using the latest "bright source" background model.

Only proportional counter unit (PCU) number 2 of the PCA (Bradt et al. 1993) detector has been used for the data extraction. We added 0.8% as a systematic error up to 7 keV and 0.4% above 7 keV (for the details of how we estimated systematic uncertainties, see Tomsick et al. [2001]).

For HEXTE, we used the response matrix created by the FTOOLS and applied the necessary dead-time correction (Rothschild et al. 1998). The HEXTE background is measured throughout the observation by alternating between the source and background fields every 32 s. The data from the background regions are merged. HEXTE channels were grouped by 2 for channels 16–31, by 4 for channels 32–59, by 10 for channels 60–99, and by 64 for channels 100–227.

[4] Available at http://heasarc.gsfc.nasa.gov/docs/xte/recipes/cook_book.html.

TABLE 2
Sources Detected by SPI in the Field of View of GX 339−4 during Revolutions 166+167

Source	Φ (23–50)	σ (23–50)	σ (50–95)	σ (95–195)
4U 1700−377	233.5 ± 6.1	38.3	11.9	5.3
4U 1630−47	85.6 ± 2.1	40.1	10.6	7.5
GX 339−4	44.2 ± 2.3	19.6	10.5	8.5
IGR J16316−4028	21.9 ± 2.8	7.9	...	...
OAO 1657−415	26.7 ± 1.9	13.6	...	...
4U 1636−536	44.4 ± 2.5	17.6	...	...
H1705−440	68.2 ± 2.2	31.0	...	...
GX 354−0	150.2 ± 5.8	25.9	6.6	...
GX 340+0	31.3 ± 2.1	14.9	...	...
1E 1740.7−2942	62.6 ± 15.9	3.9	2.2	2.2
4U 1625−33	27.5 ± 4.4	6.3	2.9	2.2

Note.—The quantity Φ is the flux in the 23–50 keV energy range, and σ is the significance in the 23–50, 50–95, and 95–195 keV energy ranges.

By fitting HEXTE data during the observation period of revolution 175 with a power-law plus cutoff model, we found a χ^2 value of 2.15 (12 degrees of freedom [dof]). All the fits, including these HEXTE points, are clearly degraded. Therefore, we suspect a problem for this particular data set (see χ^2 values in Tables 4, 5, and 6 below). Thus, we decided to perform the analysis both with and without the HEXTE data for this particular revolution. We stress that including the HEXTE data vastly degrades the χ^2 value, and thus we do not consider the corresponding results in the discussion.

3. RESULTS

3.1. *Field of View around GX 339−4: Flux Extraction*

Several hard X-ray sources are present in the GX 339−4 field and have to be carefully taken into account with appropriate variability timescales in the SPI analysis. The sources detected above 20 keV using SPIROS for revolutions 166+167 are listed with their 23–50 keV mean fluxes in Table 2.

As mentioned in § 2.1, the errors increase with the number of sources and temporal bins. So we make sure that each additional degree of freedom really does improve the χ^2. First, due to its highly variable behavior, the 4U 1700−377 light curve in the 23–200 keV energy range requires the use of the highest timescale resolution; that is, one pointing (whose duration is about 1770 s during revolution 166 and 2700 s for the others). Then timescale variabilities of a duration of three (for 4U 1630−47, GX 354−0, and GX 340+0) and two (for OAO 1657−415) pointings were found to significantly improve the values of χ^2. We consider finally six, four, and two other sources, including GX 339−4, with a constant flux for revolutions 166+167, 174, and 175, respectively.

The resulting 23–44 and 44–95 keV fluxes obtained with SPI for GX 339−4 are presented in Table 3. The quoted errors are at the 1 σ level. It appears that the source flux increases by a factor of 3 between revolutions 166+167 and revolutions 174 and 175. When going to higher energies, the sources' significances decrease (see Table 2), and we thus consider only five sources to extract fluxes above 150 keV.

3.2. *Spectral Evolution*

The GX 339−4 spectra corresponding to each set of data detailed in Table 1 have been fitted with various models available

TABLE 3
FLUX OF GX 339−4 OBSERVED BY SPI

Revolution	Φ_{23-44}	Φ_{44-95}
166+167	42 ± 2	59 ± 4
174.....	156 ± 6	211 ± 10
175.....	152 ± 6	201 ± 10

NOTE.—Flux for the data sets introduced in Table 1, in the 23–44 and 44–95 keV energy ranges (expressed in units of mcrab).

in the standard XSPEC 11.3.1 fitting package (Arnaud 1996). In all cases, we account for the interstellar absorption (PHABS in XSPEC) by using a column density $N_{\rm H}$ of 3.7×10^{21} cm^{-2} (Miller et al. 2006). In all fits, the iron emission line was modeled by a narrow Gaussian fixed at an energy of 6.4 keV. As the width of the line is only weakly constrained, it was fixed at 0.1 keV. For all models, the inner disk inclination was fixed at 50°. The data of revolutions 166 and 167 have been added together to improve statistics, due to the low flux of the source and short duration of revolution 167.

We used the simultaneous PCA (3–25 keV), HEXTE (25–200 keV), IBIS (25–200 keV), and SPI (23–600 keV) data for the spectral analysis.

3.2.1. *PEXRAV Model*

First we fitted all data with the PEXRAV model (Magdziarz & Zdziarski 1995), which consists of a power law with a high-energy cutoff and reflection from a neutral medium. Fixing the reflection fraction to $\Omega = 0$ provides a marginally acceptable fit for revolutions 166+167 (reduced χ^2 of 1.11) and a very poor description of the data for revolutions 174 and 175 (reduced χ^2 of 2.12 and 2.86, respectively). The pattern of residuals is characteristic of the presence of Compton reflection. Adding a reflection component improves the fit dramatically, reducing the χ^2 to 0.82, 0.91, and 1.09 for revolutions 166+167, 174, and 175, respectively (see Table 4). The addition of a Compton reflection gives a better fit at a high significance during all those observations, with a probability of $\lesssim 10^{-13}$ that adding this component is not required by the data (as obtained using the *F*-test).

We see in Table 4 that the reflection fraction increases and reaches a value of ∼0.5 when the flux is high. The photon index is around 1.6–1.7, as is usually observed, but the energy cutoff is rather high (300–400 keV). To test the reality of the cutoff, we perform fits with the same model but fixing E_c to 2 MeV (i.e., outside our energy range). The fit with a free high-energy cutoff is significantly better in all cases, with an *F*-test probability of 10^{-12}, 3×10^{-17}, and 2×10^{-12} for revolutions 166+167, 174, and 175, respectively. We attempted to fit with ionized reflection using the PEXRIV model, but the best-fit ionization parameter tends to zero.

3.2.2. *Physical Models Based on Comptonization*

To go more deeply into the understanding of the source behavior, we have used more sophisticated models that are based on the Comptonization process, as it is thought to be the main mechanism that is able to produce the emission observed in our energy domain.

3.2.2.1. COMPPS Model

First we modeled the X-ray and γ-ray spectrum with the thermal Comptonization model COMPPS (Poutanen & Svensson 1996). Blackbody seed photons are injected into a spherical corona of uniform optical depth τ and temperature kT, where they are Comptonized. The temperature of the blackbody component cannot be constrained and was frozen to 390 eV (Miller et al. 2006).

A fraction of the hard X-rays is scattered back into the disk where it is reflected. We consider the case of reflection from cold, neutral material with solar abundances.

As can be seen from Table 5, the temperature and the optical depth can be considered as constant, as well as the equivalent width, which was found to have a value of about 90 eV. Only the reflection fraction varies, increasing from 0.2 to 0.4 between the first two (low intensity) and the last two observations (brighter by a factor of 3).

We see from Figure 2 that the global shape of the spectrum is unchanged between revolutions 174 and 175, as well as the flux of the source (see Table 5). But in the latter, an excess of emission relative to the model appears above 200 keV. This is unexpected from the thermal model, and we thus investigated this point more deeply.

We first reconstructed the image in the 200–437 keV energy band for both revolutions 174 and 175 (Fig. 3). While the image of revolution 174 does not reveal any significant feature, the highest excess detected by SPIROS for revolution 175 coincides with the GX 339 position. Note that the distribution and the level of the residuals in both images follow the expected ones, thus allowing one to be confident in the data reduction process. We can assess that all statistical tests show a low level of systematics. Thus, the measured significance of the emission (4.6 σ) does not have to be corrected.

TABLE 4
PCA, HEXTE, SPI, AND ISGRI DATA FITTED SIMULTANEOUSLY, USING PHABS*(PEXRAV+GAUSSIAN)

Rev.	Γ	E_c (keV)	$\Omega/2\pi$	$W_{\rm Fe}$ (eV)	χ^2 (dof)	*F*-test
166+167	$1.58^{+0.02}_{-0.02}$	365^{+100}_{-67}	$0.22^{+0.06}_{-0.06}$	88^{+33}_{-29}	0.82 (172)	1.0×10^{-12}
	$1.65^{+0.01}_{-0.01}$	2000 fr	$0.35^{+0.05}_{-0.05}$	79^{+35}_{-30}	1.10 (173)	...
174.....	$1.64^{+0.02}_{-0.02}$	293^{+60}_{-41}	$0.43^{+0.08}_{-0.07}$	94^{+43}_{-36}	0.91 (114)	2.7×10^{-17}
	$1.77^{+0.01}_{-0.01}$	2000 fr	$0.80^{+0.06}_{-0.07}$	94^{+34}_{-34}	1.68 (115)	...
175.....	$1.67^{+0.02}_{-0.02}$	325^{+68}_{-50}	$0.50^{+0.08}_{-0.07}$	77^{+38}_{-36}	1.09 (100)	1.53×10^{-12}
	$1.78^{+0.01}_{-0.01}$	2000 fr	$0.85^{+0.07}_{-0.07}$	82^{+40}_{-41}	1.78 (101)	...
175*	$1.69^{+0.02}_{-0.02}$	402^{+103}_{-71}	$0.52^{+0.08}_{-0.08}$	77^{+38}_{-36}	1.60 (114)	1.94×10^{-7}
	$1.79^{+0.01}_{-0.01}$	2000 fr	$0.82^{+0.06}_{-0.05}$	72^{+34}_{-36}	2.02 (115)	...

NOTES.—The quantity Γ is the photon index, and E_c is the energy cutoff. The Gaussian line was fixed at an energy of 6.4 keV with a width fixed to 0.1 keV. The quantity $W_{\rm Fe}$ is the equivalent width, and $\Omega/2\pi$ is the reflection fraction. The *F*-test is calculated between models with free cutoff and no (i.e., fixed) cutoff. We show, for the data set of revolution 175, the fit parameters in the case for which the HEXTE data have been included (indicated as "175*").

TABLE 5
PCA, HEXTE, SPI, AND ISGRI DATA FITTED SIMULTANEOUSLY, USING PHABS*(COMPPS+GAUSSIAN)

Rev.	kT (keV)	τ	$W_{\rm Fe}$ (keV)	$\Omega/2\pi$	L_{2-600} ($\times 10^{36}$ ergs s^{-1})	y	χ^2 (dof)
166+167	72^{+21}_{-18}	$2.40^{+0.72}_{-0.64}$	87^{+28}_{-46}	$0.23^{+0.06}_{-0.06}$	$12.8^{+1.0}_{-1.0}$	1.35	0.88 (172)
174.....	64^{+10}_{-7}	$2.43^{+0.48}_{-0.53}$	91^{+31}_{-40}	$0.37^{+0.06}_{-0.05}$	$35.5^{+0.1}_{-0.2}$	1.22	0.82 (113)
175.....	61^{+12}_{-8}	$2.54^{+0.46}_{-0.48}$	90^{+30}_{-34}	$0.43^{+0.06}_{-0.06}$	$34.9^{+0.1}_{-0.3}$	1.22	1.28 (98)
175*	59^{+11}_{-7}	$2.64^{+0.44}_{-0.46}$	91^{+37}_{-35}	$0.41^{+0.06}_{-0.06}$	$34.9^{+0.1}_{-0.3}$	1.22	1.46 (113)

NOTES.—The Gaussian line was fixed at an energy of 6.4 keV, with a width fixed to 0.1 keV. The seed photon temperature $kT_{\rm seed}$ was frozen to 390 eV. The quantity $W_{\rm Fe}$ is the equivalent width, $\Omega/2\pi$ is the reflection fraction, and L_{2-600} is the luminosity of the source in the 2–600 keV energy range. We show, for the data set of revolution 175, the fit parameters in the case for which the HEXTE data have been included (indicated as "175*").

Figure 4 presents the high-energy part of the source spectrum for revolutions 174 and 175, while Figure 5 displays the data for all instruments, together with the corresponding residuals relative to the COMPPS model. They show that SPI and IBIS data are in agreement, even if the IBIS points above 200 keV are not significant. The IBIS measurement in the 200–437 keV energy band gives an 3 σ upper limit of 223 mcrab, which we compare to the SPI measurement of 218 ($\pm$47) mcrab.

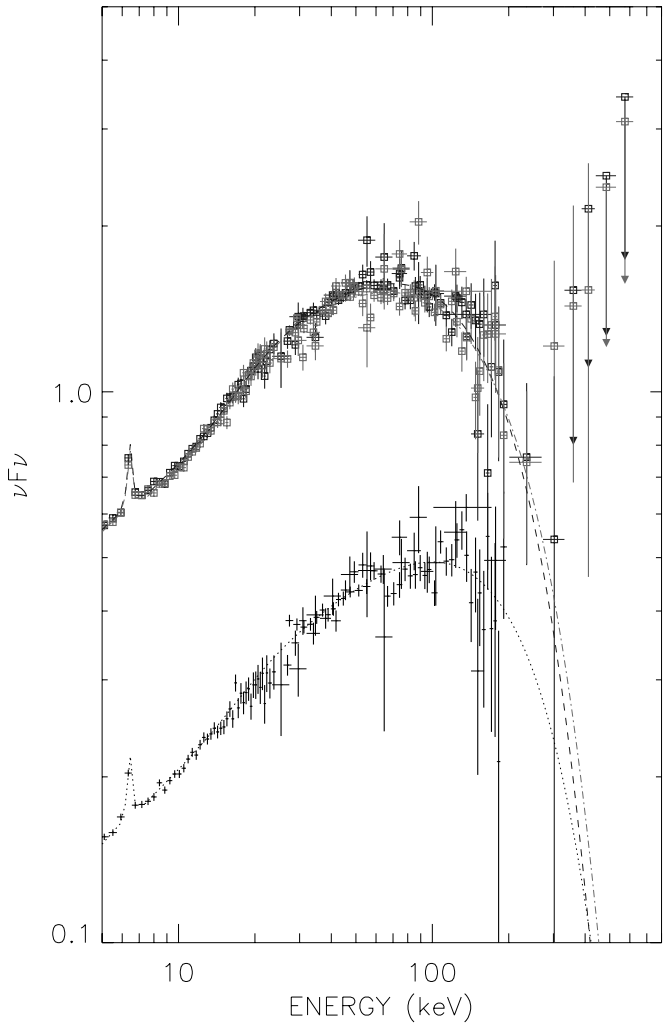

FIG. 2.—Deconvolved spectra of GX 339–4, with simultaneous PCA (3–25 keV), HEXTE (25–200 keV), SPI (23–600 keV), and ISGRI (25–518 keV) data, for revolutions 166+167 (*black plus signs*), 174 (*dark gray squares*), and 175 (*light gray squares*). The lines correspond to the best fits with the EQPAIR thermal model (see Table 6). [*See the electronic edition of the Journal for a color version of this figure.*]

We have thus used only the SPI data to quantify this excess relative to the thermal emission. The shape of the SPI spectrum during revolution 175 has been fitted using the COMPPS model. The best-fit parameters are an electron temperature kT of 44 keV and an optical depth of 4.4 (with a reduced χ^2 of 1.35). We found that the addition of a simple power law leads to an improvement of the fit of the SPI data that is significant at the 90% level according to an F-test, with a best-fit photon index of 1.07.

3.2.2.2. EQPAIR Model

We finally applied the hybrid thermal/nonthermal Comptonization model EQPAIR (Coppi 1999). This model assumes a spherical plasma cloud with isotropic and homogeneous distribution of electrons, positrons, and soft seed photons within the plasma. The properties of the plasma depend on its compactness $l = L\sigma_{\rm T}/Rm_e c^3$, where L is the power of the source, R is the radius of the sphere, which is assumed to be 10^7 cm, and $\sigma_{\rm T}$ is the Thomson cross section. We use a hard compactness l_h, which corresponds to the power supplied to the electrons, and a soft compactness l_s, corresponding to the power supplied in the form of soft seed photons. The amount of heating of the Comptonizing medium is specified through the ratio of the compactnesses of the Comptonizing medium l_h and the seed photon distribution, l_h/l_s, with l_s fixed to 1. The seed photon blackbody temperature $kT_{\rm seed}$ is frozen to 390 eV. The reflection component is modeled as in COMPPS, and the reflection fraction of $\Omega/2\pi$ obtained from the fit corresponds to the unscattered part of the Compton reflection component. The total optical depth, $\tau_{\rm tot}$, is the sum of the optical depth of e^+e^- pairs ($\tau_{e^+e^-}$) and of e^- coming from ionization of atoms ($\tau_{\rm es}$). The fitted parameters are l_h/l_s (which is related to the coronal temperature) and the ionization electron optical depth, $\tau_{\rm es}$.

In order to consider the case of a hybrid plasma, the model contains an additional parameter: the ratio $l_{\rm nth}/l_{\rm th}$, where $l_{\rm nth}$ is the compactness corresponding to the nonthermal and $l_{\rm th}$ to the thermal part of the e^+e^- distribution. The rate at which nonthermal electrons appear in the source is assumed to be a power law, $\gamma^{-\gamma_{\rm inj}}$, between the Lorentz factors $\gamma_{\rm min} = 1.3$ and $\gamma_{\rm max} = 1000$. The quantity $\gamma_{\rm inj}$ is assumed to be equal to 2. We combined EQPAIR with a Gaussian iron line centered and fixed at 6.4 keV with a width of 0.1 keV. Table 6 shows the evolution of the best-fit parameters.

We first fixed the compactness of the nonthermal electrons to zero in order to consider the case of a purely thermal plasma. Spectra extracted during all the observations are well fitted with $\chi^2 \simeq 0.8$–1.1. The hard-to-soft compactness ratio is in the range

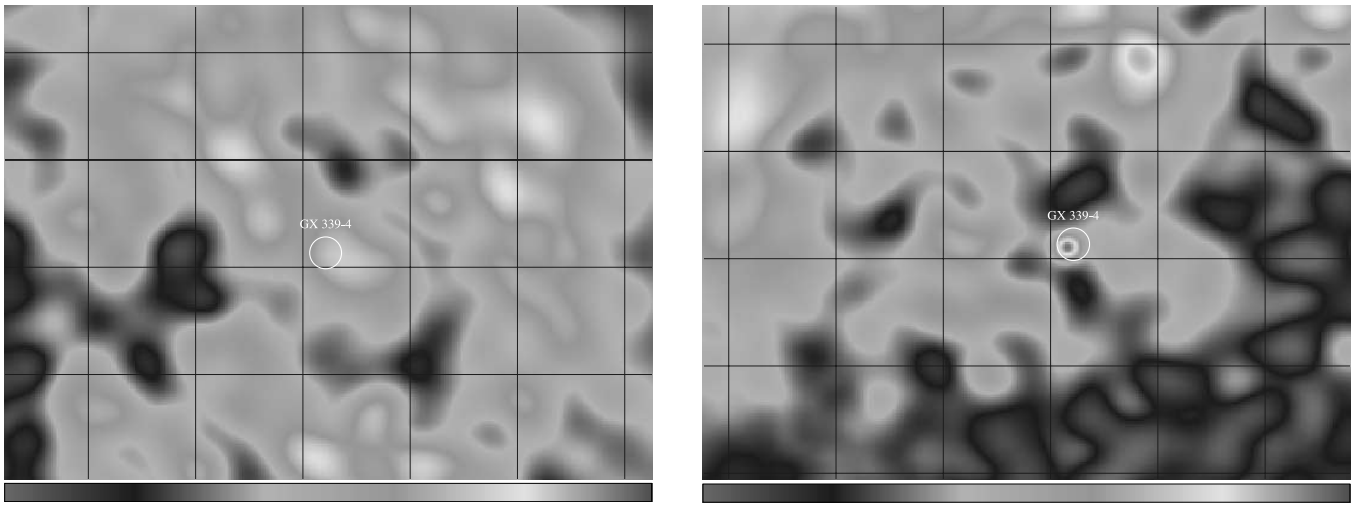

FIG. 3.—Significance maps obtained with SPIROS in the 200–437 keV energy range; the gray scale is from $-3\ \sigma$ to $4.5\ \sigma$; the grid spacing is 5°. *Left*: Revolution 174. The significance of the GX 339−4 flux is below $1.5\ \sigma$. *Right*: Revolution 175. GX 339−4 is the only significant source in the field of view detected with a flux of 193.4 ± 46.6 mcrab ($4.2\ \sigma$). [*See the electronic edition of the Journal for a color version of this figure*.]

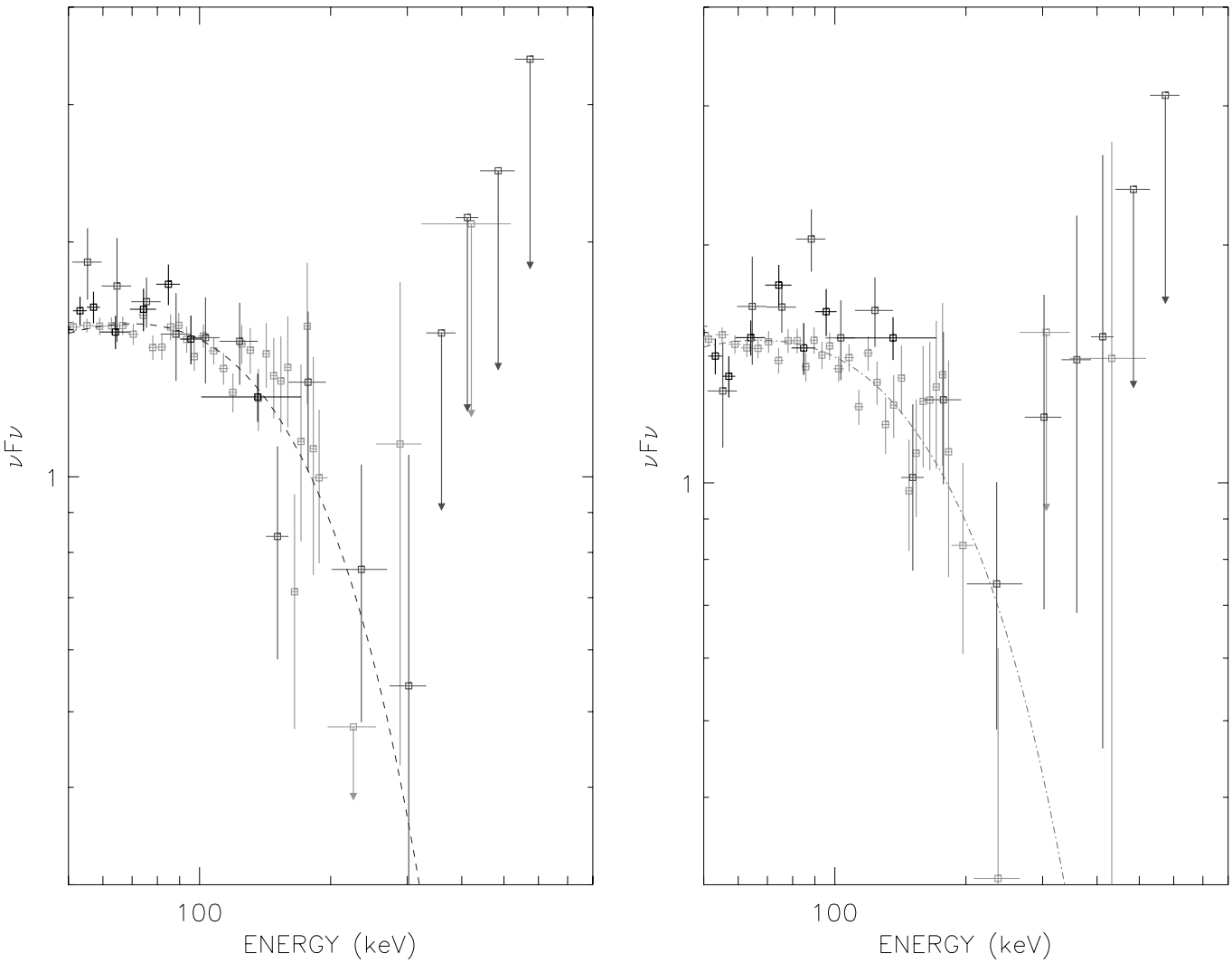

FIG. 4.—High-energy part of the GX 339−4 deconvolved spectra for revolution 174 (*left*) and for revolution 175 (*right*), with data from HEXTE (*black squares*), SPI (*dark gray squares*), and ISGRI (*light gray squares*). The line corresponds to the best fit with the EQPAIR thermal model (see Table 6). [*See the electronic edition of the Journal for a color version of this figure*.]

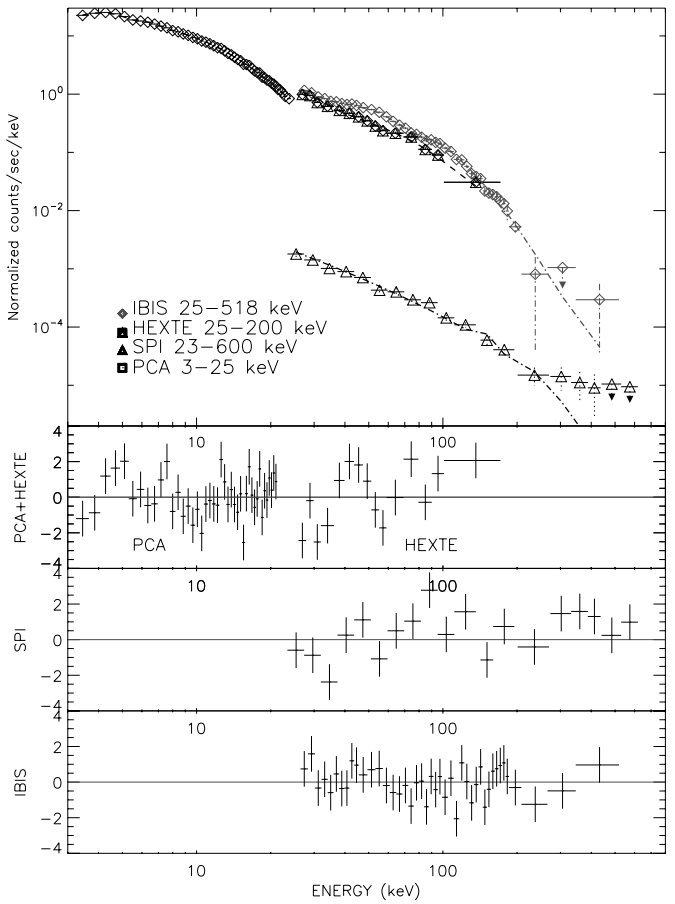

FIG. 5.—Spectra of GX 339−4 with simultaneous PCA, HEXTE, ISGRI, and SPI data for revolution 175. The COMPPS model used is described in Table 5. The residuals obtained for each instrument are presented in the lower panels. [*See the electronic edition of the Journal for a color version of this figure.*]

of 5–6, yielding a coronal temperature of about 65 keV, given the fitted optical depth of 1.6 in revolutions 174–175, while the kT (98 keV) and $\tau_{\rm tot}$ (1.1) parameters of revolutions 166+167 are very different. Part of the difference between the kT and τ best-fit values can be explained by the fact that the Comptonization model suffers from a degeneracy in their determination due to low statistics. Indeed, the spectral slope depends only on the Compton parameter $y = 4kT\tau/m_e c^2$, which does not vary a lot along the observations (see Table 6). In fact, if we freeze the optical depth in revolutions 166+167 to the value obtained in revolution 174, we obtain an acceptable χ^2 value, and the difference in temperature between both revolutions decreases. Nevertheless, the y-parameter seems to be larger in revolutions 166+167, which is confirmed by a significantly higher value of l_h/l_s. The reflection component fraction is similar to the value found with the COMPPS model, and the iron line equivalent widths are still about 90 eV.

In a second step, the compactness of the nonthermal distribution has been freed in order to consider the case of an hybrid plasma. For revolution 174, this leads to a thicker ($\tau_{\rm tot} \simeq 2.0$) and cooler ($kT_e \simeq 50$ keV) solution, relative to the thermal case, with both solutions being equivalent from a statistical point of view. Moreover, when determining the confidence range of the $l_{\rm nth}/l_{\rm th}$ parameter, we found it unconstrained, forbidding any conclusion.

The situation seems different for revolution 175, as the introduction of a nonthermal component allows a slight improvement of the value of χ^2 (with an F-test probability of 10^{-2}), even though the nonthermal fraction is not really constrained. However, the parameters are the same as in the thermal case, except the hard compactness, which slightly increases.

4. DISCUSSION

4.1. *Comparison with Previous Observations*

Broadband X-ray and γ-ray spectra of GX 339−4, using data collected from the SPI, IBIS, HEXTE, and PCA instruments, allowed us to follow the source behavior during the low/hard state corresponding to the rising phase of its 2004 outburst. During this period we observed a flux increase by a factor of 3 in the whole energy domain (3–200 keV) without any major change in the spectral shape (see Fig. 2). This is similar to results from previous outbursts reported by Zdziarski et al. (2004, their Fig. 4) where, during the LHS, in the rising phase, the source flux increases at constant spectral slope.

4.1.1. *High-Energy Cutoff and the Reflection Component*

We have showed that both a reflector and a high-energy cutoff in the primary emission component were required to describe the spectral shape during the LHS, as typically observed for GX 339−4. Simultaneous fits from PCA, HEXTE, IBIS, and SPI data give photon indexes Γ in the range of 1.6–1.7, with cutoff energies around 300–400 keV. The amplitude of the reflection component reaches similar values to those reported by Revnivtsev et al. (2001), who modeled the low/hard state of GX 339−4 during

TABLE 6
PCA, HEXTE, SPI, AND ISGRI DATA FITTED SIMULTANEOUSLY, USING THE EQPAIR MODEL COMBINED WITH A GAUSSIAN IRON LINE

Rev.	l_h/l_s	$l_{\rm nth}/l_{\rm th}$	$\tau_{\rm es}$	$W_{\rm Fe}$ (eV)	$\Omega/2\pi$	$\tau_{\rm tot}$	kT (keV)	y	χ^2 (dof)
166+167	$5.74^{+0.19}_{-0.32}$	0 fr	$1.15^{+0.05}_{-0.11}$	77^{+30}_{-40}	$0.30^{+0.03}_{-0.04}$	1.15	98	0.88	0.94 (173)
	$6.32^{+0.10}_{-0.10}$	0 fr	1.60 fr	83^{+50}_{-46}	$0.26^{+0.03}_{-0.03}$	1.60	72	0.90	0.98 (174)
174.....	$5.08^{+0.17}_{-0.12}$	0 fr	$1.61^{+0.08}_{-0.07}$	97^{+50}_{-35}	$0.42^{+0.03}_{-0.03}$	1.61	64	0.81	0.82 (114)
	$6.35^{+0.88}_{-1.11}$	$0.40^{+0.3}_{-0.3}$	$1.98^{+0.14}_{-0.18}$	102^{+50}_{-50}	$0.39^{+0.04}_{-0.04}$	2.00	50	0.78	0.82 (113)
175.....	$5.09^{+0.13}_{-0.05}$	0 fr	$1.66^{+0.06}_{-0.03}$	90^{+30}_{-50}	$0.43^{+0.03}_{-0.03}$	1.60	64	0.80	1.10 (99)
	$5.61^{+2.15}_{-0.16}$	$0.28^{+0.45}_{-0.17}$	$1.54^{+0.49}_{-0.12}$	90^{+30}_{-50}	$0.47^{+0.05}_{-0.06}$	1.56	64	0.78	1.06 (98)
175*	$5.08^{+0.17}_{-0.12}$	0 fr	$1.61^{+0.07}_{-0.02}$	90^{+36}_{-50}	$0.42^{+0.03}_{-0.04}$	1.61	64	0.81	1.47 (114)
	$7.08^{+0.46}_{-0.42}$	$0.65^{+0.17}_{-0.14}$	$1.92^{+0.15}_{-0.07}$	94^{+92}_{-59}	$0.45^{+0.06}_{-0.05}$	1.93	50	0.76	1.45 (113)

NOTES.—See text for the description of the parameters. The quantity $kT_{\rm seed}$ has been frozen to 390 eV, with an inclination angle of 50°. Both $\tau_{\rm tot}$ and kT are calculated from fitted parameters. We show, for the data set of revolution 175, the fit parameters in the case for which the HEXTE data have been included (indicated as "175*").

its outbursts of 1996–1997 as observed by the PCA. They found photon indexes Γ in the range of 1.7–1.9 and a reflection amplitude of 0.3–0.5. Moreover, the reflection fraction increases with the photon index of the power law and flux in a way similar to the correlation already observed by Nowak et al. (2002) for GX 339−4 and in a large sample of Seyfert and X-ray binaries by Zdziarski et al. (1999, 2003). Zdziarski et al. (1999) have interpreted the Ω-Γ correlation as being due to feedback in an inner hot (thermal) accretion flow surrounded by an overlapping cold disk. Then, the closer to the central black hole the cold disk extends, the more cooling of the hot plasma by blackbody photons occurs (indicated by the decrease of the electron temperature kT fitted by the COMPPS model), and the softer the spectrum becomes (as shown from the power-law slope Γ fitted by the PEXRAV model).

4.1.2. *Comptonization Parameters*

We then introduced the physical models COMPPS and EQPAIR to describe the GX 339−4 observations with the Comptonization process. From a statistical point of view, both models give acceptable solutions. Data from revolutions 166+167 and 174 are well fitted with the Comptonization model in a purely thermal case, while the last revolution suggests the presence of a nonthermal component.

Wardziński et al. (2002) modeled the outburst of 1991 September observed by the *Ginga* LAC and the *CGRO* OSSE, as well as the outbursts of 1996 and 1997 observed by the *RXTE* PCA and HEXTE with the COMPPS model. The Comptonization spectrum was characterized by Thomson optical depths τ of 2.4–3.0 and an electron temperature of 60 keV. The reflection component was found to be moderately ionized, with amplitudes ranging from 0.2 to 0.4. We have tested the ionized case, but the ionization parameter tends to zero. We have thus fixed it to zero and in fact have deduced very similar best-fit parameters.

The EQPAIR thermal model has been used by Nowak et al. (2002) to interpret the spectra obtained during the low/hard state observations of the GX 339−4 outbursts in 1997 and 1999 by PCA and HEXTE. With a fitted seed photon temperature of 30–100 eV, they found coronal compactnesses l_c ranging from 5 to 14 and electron optical depths $\tau_{\rm es}$ ranging from 0.01 to 0.6, yielding total optical depths $\tau_{\rm tot}$ between 0.1 and 1 and values of kT_e around 200 keV. The reflection fractions are between 0.1 and 0.5, and the equivalent widths of the iron line range from 80 to 240 eV. We find similar values for the reflection fraction, the iron line width, and the coronal compactness, but with thicker ($\tau_{\rm tot}$ around 1.6–1.7) and colder (kT_e around 65 keV) plasma parameters.

4.2. *The High-Energy Excess*

An interesting feature appears in the SPI data at revolution 175 as the emission extends beyond the thermal cutoff. Such an excess above 200 keV has already been observed by the OSSE instrument (Johnson et al. 1993) in the low/hard state of the GX 339−4 outburst event in 1991 September. Assuming a distance of 6 kpc, the luminosity above 200 keV was 11.3×10^{36} ergs s^{-1} (Johnson et al. 1993), with a 35–300 keV luminosity $L_{35-300\ \rm keV}$ of 2.5×10^{37} ergs s^{-1}. These values are comparable to what we found for the excess observed during revolution 175, with a luminosity above 200 keV of $7.2 \pm 1.6 \times 10^{36}$ ergs s^{-1} and $L_{35-300\ \rm keV} \simeq 1.54 \times 10^{37}$ ergs s^{-1}. More recently, a similar feature has been reported in one *RXTE* observation (Nowak et al. 2002), where the HEXTE spectrum exhibits a hardening above $\sim$100 keV. Similar behavior is observed for Galactic black hole transients in the LHS during the outburst decays, especially after the detection of compact jets (Kalemci et al. 2005, 2006).

The flux extension above a thermal Comptonization component can be explained by a second Comptonization region/population or, more or less equivalently, spatial (gradient) and/or temporal variations in the plasma parameters. As our fitting models assume them to be homogeneous and constant during one observation, such variations can produce deviation relative to the predicted spectrum. Another possibility could be the presence of a large annihilation line, which would produce a bump extending down to 250–300 keV. Alternatively, some models include the presence of a nonthermal electron population in the plasma. The high-energy power-law tail observed for Cyg X-1 in its LHS has been modeled with hybrid Comptonization by injecting an electron population consisting of a Maxwellian distribution coupled to a power law with an index of 4.5 (McConnell et al. 2000). The presence of a high-energy electron tail has also been proposed by Wardziński et al. (2002) for simultaneous observations of GX 339−4 with PCA+HEXTE and *CGRO* OSSE during the outburst of 1997, even though the COMPPS model fits the data reasonably well. They found that the introduction of a nonthermal fraction of electrons improves the value of χ^2, and it corresponds to 34% of the nonthermal emission.

The EQPAIR hybrid plasma allows a marginally better description of the spectrum during revolution 175. Adding a nonthermal parameter $l_{\rm nth}$ to the purely thermal plasma case gives an F-test value of about 10^{-2}. However, the value of the $l_{\rm nth}/l_{\rm th}$ fraction ($\simeq$0.28) is similar to the value found for the LHS of GX 339−4 by Wardziński et al. (2002), even though these values are in fact not constrained.

In Galactic black holes, nonthermal emission is generally associated with the soft state (Grove 1999; Ling et al. 1994) or with state transitions (see, e.g., Cadolle Bel et al. 2006; Malzac et al. 2006), where power-law tails are observed and are attributed to Comptonization of soft photons by accelerated electrons. During the transition from the low/hard to the high/soft state on 2003 August 15, Belloni et al. (2006) observed that the high-energy cutoff increases/disappears.

In the LHS, the hard X-ray/γ-ray emission comes from a thermalized electron population. The presence in the low/hard state of a significant nonthermal emission above the thermal cutoff can, however, be interpreted in terms of an additional component. Contrary to the soft state, in which power-law tails are commonly observed, this characteristic is much rarer in the LHS. In our observations, this feature is detected only in one revolution; nevertheless, the statistic is not high enough to conclude on its variability. Moreover, as the low-energy part of the spectrum is not affected (the spectral shape is similar up to $\simeq$150 keV in revolutions 174 and 175), this may suggest that the involved phenomenon varies independently of the thermal Comptonization process and could come from another location, such as jets or active regions. A jet can easily produce hard X-ray emission via synchrotron radiation, in addition to inverse Compton upscattering (see, e.g., Markoff et al. 2003).

5. CONCLUSIONS

We investigated the high-energy spectral characteristics of GX 339−4 in the low/hard state (the rising phase of the outburst), using observations from *INTEGRAL* SPI and IBIS and *RXTE* PCA and HEXTE. The plasma parameters deduced from thermal Comptonization models are identical to those obtained during previous observations performed when the source was in a similar spectral state, with a plasma temperature kT of around 65 keV, an optical depth $\tau \simeq 1.5$–2.5, and a reflection factor lower than 1 (0.2–0.4), supporting an anisotropic primary emission or a large value of the disk internal radius. An emission in excess

relative to the thermal cutoff has been detected during one revolution, despite being absent 3 days before. The corresponding flux (typically emission above 200 keV) is not highly significant, with only 4.6 σ, but can be compared to features reported by OSSE and HEXTE in GX 339−4 or Cyg X-1. This may be evidence that an additional component is sometimes present in the spectrum, unless variabilities (spatial and/or temporal) of the kT and τ plasma parameters can mimic such spectral evolution affecting only the energy domain above 200 keV.

The SPI project has been completed under the responsibility and leadership of the CNES. We are grateful to ASI, CEA, DLR, ESA, INTA, NASA, and OSTC for support.

Specific software packages used for this work have been developed by L. Bouchet. E. K. acknowledges partial support from TUBITAK and Marie Curie International Reintegration grant MIRG-CT-2005-017203. The authors are grateful to the anonymous referee for their very fruitful comments that allowed us to improve the quality of this paper.

REFERENCES

Arnaud, K. A. 1996, in ASP Conf. Ser. 101, Astronomical Data Analysis Software and Systems V, ed. G. H. Jacoby & J. Barnes (San Francisco: ASP), 17
Baluncinska-Church, M., Belloni, T., Church, M. J., & Hasinger, G. 1995, A&A, 302, L5
Belloni, T., Homan, J., Casella, P., van der Klis, M., Nespoli, E., Lewin, W. H. G., Miller, J. M., & Méndez, M. 2005, A&A, 440, 207
Belloni, T., Homan, J., Cui, W., & Swank, J. 2004, ATel, 236
Belloni, T., et al. 2006, MNRAS, 367, 1113
Bouchet, L., et al. 1993, ApJ, 407, 739
Bradt, H. V., Rothschild, R. E., & Swank, J. K. 1993, A&AS, 97, 355
Buxton, M., Gallo, E., Fender, R., & Bailyn, C. 2004, ATel, 230
Cadolle Bel, M., et al. 2006, A&A, 446, 591
Chaty, S., Haswell, C. A., Malzac, J., Hynes, R. I., Shrader, C. R., & Cui, W. 2003, MNRAS, 346, 689
Coppi, P. S. 1999, in ASP Conf. Ser. 161, High Energy Processes in Accreting Black Holes, ed. J. Poutanen & R. Svensson (San Francisco: ASP), 375
Corbel, S., & Fender, R. P. 2002, ApJ, 573, L35
Fender, R. P. 2006, in Compact Stellar X-Ray Sources, ed. W. H. G. Lewin & M. van der Klis (Cambridge: Cambridge Univ. Press), 381
George, I. M., & Fabian, A. C. 1991, MNRAS, 249, 352
Gierliński, M., Zdziarski, A. A., Done, C., Johnson, W. N., Ebisawa, K., Ueda, Y., Haardt, F., & Phlips, B. F. 1997, MNRAS, 288, 958
Grabelsky, D. A., et al. 1993, BAAS, 25, 1337
Grebenev, S., et al. 1993, A&AS, 97, 281
Grove, J. E. 1999, in ASP Conf. Ser. 161, High Energy Processes in Accreting Black Holes, ed. J. Poutanen & R. Svensson (San Francisco: ASP), 54
Homan, J., Buxton, M., Markoff, S., Bailyn., C. D., Nespoli, E., & Belloni, T. 2005, ApJ, 624, 295
Hynes, R. I., Steeghs, D., Casares, J., Charles, P. A., & O'Brien, K. 2003, ApJ, 583, L95
Jensen, P. L., Clausen, K., Cassi, C., Ravera, F., Janin, G., Winkler, C., & Much, R. 2003, A&A, 411, L7
Johnson, W. N., et al. 1993, A&AS, 97, 21
Joinet, A., et al. 2005, ApJ, 629, 1008
Kalemci, E., Tomsick, J. A., Buxton, M. M., Rothschild, R. E., Pottschmidt, K., Corbel, S., Brocksopp, C., & Kaaret, P. 2005, ApJ, 622, 508
Kalemci, E., Tomsick, J. A., Rothschild, R. E., Pottschmidt, K., Corbel, S., & Kaaret, P. 2006, ApJ, 639, 340
Kong, A. K. H., Charles, P. A., Kuulkers, E., & Kitamoto, S. 2002, MNRAS, 329, 588
Kuulkers, E., et al. 2004, ATel, 240
Lebrun, F., et al. 2003, A&A, 411, L141
Ling, J. C., Wheaton, Wm. A., Skelton, R. T., Harmon, B. A., Rubin, B. C., Fishman, G. J., & Paciesas, W. S. 1994, BAAS, 26, 971
Magdziarz, P., & Zdziarski, A. A. 1995, MNRAS, 273, 837
Malzac, J., et al. 2006, A&A, 448, 1125
Markert, T. H., Canizares, C. R., Clark, G. W., Lewin, W. H. G., Schnopper, H. W., & Sprott, G. F. 1973, ApJ, 184, L67
Markoff, S., Nowak, M., Corbel, S., Fender, R., & Falcke, H. 2003, A&A, 397, 645
McClintock, J. E., & Remillard, R. A. 2006, in Compact Stellar X-Ray Sources, ed. W. H. G. Lewin & M. van der Klis (Cambridge: Cambridge Univ. Press), 157
McClintock, J. E., et al. 2001, ApJ, 555, 477
McConnell, M. L., et al. 2000, ApJ, 543, 928
Miller, J. M., Homan, J., Steeghs, D., Rupen, M. Hunstead, R. W., Wijnands, R., Charles, P. A., & Fabian, A. C. 2006, ApJ, 653, 525
Miller, J. M., et al. 2004a, ApJ, 601, 450
———. 2004b, ApJ, 606, L131
Nowak, M. A., Wilms, J., & Dove, J. B. 2002, MNRAS, 332, 856
Poutanen, J., & Svensson, R. 1996, ApJ, 470, 249
Remillard, R. A. 2005, in Proc. 22nd Texas Symposium on Relativistic Astrophysics, ed. P. Chen et al. (eConf C041213; Stanford: Stanford Univ.), http://www.slac.stanford.edu/econf/C041213/
Revnivtsev, M., Gilfanov, M., & Churazov, E. 2001, A&A, 380, 520
Rodriguez, J., et al. 2006, MNRAS, 366, 274
Roques, J. P., et al. 2003, A&A, 411, L91
Rothschild, R. E., et al. 1998, ApJ, 496, 538
Shahbaz, T., Fender, R., & Charles, P. A. 2001, A&A, 376, L17
Smith, D. M., Heindl, W. A., Swank, J. H., Wilms, J., & Pottschmidt, K. 2004, ATel, 231
Sturner, S. J., et al. 2003, A&A, 411, L81
Tomsick, J. A., Corbel, S., & Kaaret, P. 2001, ApJ, 563, 229
Vedrenne, G., et al. 2003, A&A, 411, L63
Wardziński, G., Zdziarski, A. A., Gierliński, M., Grove, J. E., Jahoda, K., & Johnson, W. N. 2002, MNRAS, 337, 829
Zdziarski, A. A., Gierliński, M., Mikolajewska, J., Wardziński, G., Smith, D. M., Alan, H. B., & Kitamoto, S. 2004, MNRAS, 351, 791
Zdziarski, A. A., Lubiński, P., Gilfanov, M., & Revnivtsev, M. 2003, MNRAS, 342, 355
Zdziarski, A. A., Lubiński, P., & Smith, D. A. 1999, MNRAS, 303, L11